

High-selectivity single-chip spectrometer in silicon for operation at visible part of the spectrum

J. H. Correia, M. Bartek and R. F. Wolffenbuttel

Delft University of Technology, ITS/Electrical Engineering

Lab. for Electronic Instrumentation/DIMES

Mekelweg 4, 2628 CD, Delft, The Netherlands

Phone: +31-15-2781602, Fax: +31-15-2785755, E-mail: J.H.Correia@its.tudelft.nl

Abstract

A microspectrometer has been realized based on an array of Fabry-Perot optical thin film filters. The 16-channel microspectrometer is compatible with IC fabrication methods and operates in the visible spectral range with an inter-channel shift of 6 nm. Each of the channels is sensitive in a single peak with Full-Width-Half-Maximum (FWHM) of 16 nm. Also a FWHM below 2 nm and finesse of 40 for narrow band operation is demonstrated. The device can easily be tuned during fabrication to cover a different spectral band only by adjusting the etching times without affecting the device layout. Such a device is extremely suitable for applications in microsystems because of its small size, high spectral selectivity and low cost. Microspectrometers for the UV and IR regions are also feasible using this technique.

Keywords: Array-type microspectrometer, Fabry-Perot etalon, visible light detector, optical filter, FWHM, finesse.

I. INTRODUCTION

Conventional benchtop spectrometers involve a complex system of lenses and moving parts (or a high-density photodetector array), and are thus bulky and expensive. By applying micromachining techniques one may be able to produce a spectrometer with drastically reduced size and costs (in high-volume production). In addition, a number of these systems can be combined for improved spectral range and/or resolution. Moreover, an integrated optical device has a number of advantages over a conventional optical system, such as a simplified assembly, stable alignment, and compact size.

The dimensional advantage of a miniaturized spectrometer is, in many applications, of higher importance than its reduced resolution. For example, examination of products in a manufacturing line by means of laboratory analysis is time consuming, increases costs and sometimes stops production. Therefore, it has become important to perform on-line measurements in the process line in order to correct any process problems in real time. A small spectrometer offers a huge potential to serve the needs of future automated optical inspection systems.

Identification of the composition of gases and liquids, chemical analysis by optical absorption, emission-line characterization, colorimetry and biochemical analysis are some of the applications where a miniaturized spectrometer can be useful [1].

Previously developed microspectrometers [2-6], fabricated using bulk or surface micromachining, contain movable parts to perform wavelength tuning. As a result, they have limited reliability and are suitable only for operation in a limited spectral band (mostly near-IR) [6,7]. Moreover, high-voltage electrostatic actuation is necessary for resonance cavity tuning.

Operation in the visible spectral range (with a single transmission peak) implies a maximum cavity length of 400 nm. Fabrication and modulation of such a narrow airgap between the two mirrors is severely hindered by capillary forces inside of the cavity. Also, electrostatic pull-in and subsequent sticking of the two mirrors limits the operating range of the device to one third

of the initial air gap [8]. Small resolution ($R=\lambda/\Delta\lambda$, with $\Delta\lambda$ the smallest wavelength difference distinguishable at a specific wavelength, λ) are a limitation of microspectrometers because the optical path length available is short (especially in grating-based microspectrometers) compared with the large dimensions systems.

II. MICROSPECTROMETER DESIGN

A. *The complete structure*

A new single-chip, Fabry-Perot array-type microspectrometer was developed. This device is suitable for operation in the visible spectral range and does not require electrostatic actuation. The Fabry-Perot structure is a simple interferometer where the incident light suffers multiple reflections between the coated surfaces that define the cavity. The emerging wavefronts interfere constructively only if there is no phase difference between them. At other wavelengths, destructive interference of the transmitted wavefronts reduces the transmitted intensity towards to zero. Therefore, this device acts as a filter that transmits certain wavelengths and reflects the others back to the light source.

The realized microspectrometer, shown schematically in Fig. 1 (an individual channel in cross-section) and Fig. 2 (the complete 4x4 array microspectrometer), is fully compatible with standard IC processing methods.

The impinging spectrum is filtered in the Fabry-Perot resonator and the intensity of the selected spectral component is measured in transmission using an underlying integrated photodiode array. On top of each photodiode a deposited Al/SiO₂/Ag layer stack functions as a Fabry-Perot optical filter. The thickness of the PECVD-silicon-dioxide layer, which is enclosed between two semi-transparent metallic mirrors, determines the wavelength tuned to. In N subsequent plasma etching steps (using different photoresist masks), the initially deposited PECVD oxide layer is thinned forming 2^N channels, each with a different resonance cavity length. An oxide layer is

present between the cavity and the photodiode and introduces a wavelength-dependent transmission of the incident radiation. Its thickness was designed to yield a flat transmittance over the visible spectral range (approximately 50 nm) [9-10]. Evaporated metallic mirrors were used instead of high-performance dielectric mirrors, to maintain fabrication simplicity (only one layer must be deposited).

Another advantage of metallic mirrors is the suitability for use over a wide spectral range [11]. Silver and aluminum have been selected for high reflectivity at visible wavelengths (see Fig. 3). Fabry-Perot filters using metallic mirrors cannot provide both high finesse (ratio between the free spectral range and FWHM) and high transmittance simultaneously due to the optical absorption in the metal layers (Fig. 4). Unlike macroscopic applications of silver-based reflective coatings [12], the poor environmental resistance of silver is not critical in a microsystem application. Sealing of a complete system avoids any environmentally induced mirror degradation.

B. Selection of materials

According to the simulation results, the best option for a Fabry-Perot resonance cavity for the visible range in terms of optical characteristics is to use silver mirrors (higher reflectance than aluminum mirrors) with an intermediate air gap (lowest refractive index). Because the array type has fixed cavities of different widths, an array of Fabry-Perot etalons (cavity medium different from air) was implemented. In conventional devices, it is common to use a dielectric film such as glass or silica as cavity medium. Two different dielectric materials were investigated: silicon nitride (Si_xN_y) and PECVD silicon dioxide (SiO_2). Si_xN_y films are characterized by stronger dispersion and larger values of the refractive index. The dependence of refractive index on the wavelength for the PECVD SiO_2 films is more constant (varies from 1.47 to 1.46 between 400 nm to 800 nm wavelengths) [9]. Therefore, PECVD SiO_2 was selected.

Due to fabrication constraints, the bottom mirror of the etalon is a thin aluminum film instead of silver (a soft metal for evaporation). Only the top mirror is a thin film of silver deposited at the last step in the fabrication process. The compatibility with standard microelectronics processing implies that only Si-compatible materials should be used, avoiding contamination of the process with the deposition of silver in an intermediate step.

C. Optical simulations of the Fabry-Perot etalon

A thin-film optics software package -TFCalc v.3.2 (from Software Spectra)- was used for structural optimization of the Fabry-Perot filter. The transmittance of a 60 nm-Ag/1000 nm-SiO₂/60 nm-Ag layer stack (Fig. 5) shows a FWHM of 1.8 nm and a finesse of 40. The Ag-layer thickness is a trade-off between achievable FWHM and absorption loss. When aluminum is used for the bottom mirror (due to fabrication constraints), the performance slightly decreases due to higher absorption and less reflectance of aluminum films compared to that of silver films.

D. Phototransducers

Each channel in the microspectrometer is composed of a Fabry-Perot etalon with an optical detector underneath. The detector is a p-n junction photodiode fabricated in a standard bipolar process (see Fig. 1). The absorption of light in silicon is wavelength dependent: long wavelength light penetrates much deeper before being absorbed.

Junction isolation using deep boron diffusions electrically separates individual photodiodes (see Fig. 1). The top surface between different channels is covered with metal in order to shield from stray light.

Limiting factors in the opto-electrical conversion in a photodiode are the size and uniformity of the effective sensing area and dark current. Dark current is the current that flows in a photodiode when there is no optical radiation incident on the photodiode. Compensation techniques are usually employed to minimize this effect. As the dark current is temperature dependent, one meas-

urement at the beginning of the experiment is usually not sufficient. A dark-current-compensation channel is implemented using a photodiode completely covered with metal.

The dominant noise source in a photodiode is shot noise [13]. Another form of noise is the fixed pattern noise. It is defined as the photoresponse variation between adjacent photodiodes. The fixed pattern noise is controlled by the size of the photodiode relative to the minimum lithographic feature size. As the dimensions of the photodiodes (1 mm^2) are relatively large, this noise is negligible [14], less than 1% in our case.

The cross-talk resulting from photon-produced minority-carrier diffusion is a problem in optical detection with more than one channel. The carriers generated outside the junction depletion layer may diffuse to a neighbouring photodiode and thus introduce an undesired current component. In certain silicon processes the diffusion length of such carriers can be up to $100 \text{ }\mu\text{m}$ [15]. So, this minority-carrier diffusion causes cross-talk in a closely-spaced photodiode array. Moreover, the problem cannot be resolved by a light shield, because the carriers are primarily produced under a photodiode. The solution is to form a deep p-diffusion that contacts the p-substrate and is connected to ground potential (junction isolation). In this way the photocurrent in a diode is contributed to only by the photocarriers generated in or near the depletion layer between the p-diffusion and the n-diffusion regions. Minority carriers generated above or below the n-diffusion/p-substrate junction or diffusing from neighbouring photodiodes, will be swept away from the n-diffusion region by the junction field, or be bypassed to the power supply.

III. DEVICE FABRICATION

The photodiode array was fabricated using a bipolar process in silicon [16]. The Fabry-Perot etalons were added in a post-process module. The post-process module, which was used to fabricate the 16 etalons, each with a different thickness, requires further explanation. The formation of the Fabry-Perot etalon starts with the deposition of a 20 nm Al layer after completion of the

bipolar process (including metallization and thinning of the oxide above the photodiodes). The oxide passivation layer on top of the photodetector (between the Fabry-Perot etalon and Si substrate surface) is thinned to reduce its influence on the spectral response. The thin Al layer is evaporated and patterned using lift-off. Subsequently, a PECVD oxide layer is deposited with a thickness equal to the maximum cavity length (300 nm in this example). The thickness of the PECVD silicon dioxide layer, which is enclosed between two semi-transparent metallic mirrors, determines the wavelength for tuning. In N subsequent plasma etching steps (for which different photoresist masks are used), the initially deposited PECVD oxide layer is thinned that 2^N channels are formed, each with a different resonance cavity length. An example with four masks for a 4x4 array-type microspectrometer is shown in Fig. 6. After the deposition of the silicon dioxide, each mask used has a different etching time (T, T/2, T/4, T/8). A relative thickness uniformity better than 2 nm was achieved between cavity lengths. A silver layer is deposited at the very end of the fabrication sequence and patterned using lift-off. Fig. 7 presents a complete description of the bipolar post-processing fabrication sequence. Fig. 8 shows a SEM photograph presenting the cross section of one of the channels. Fig. 9 shows a photograph of the fabricated device with overall dimensions of $4.7 \times 4.7 \text{ mm}^2$.

IV. EXPERIMENTAL RESULTS

The electrical characteristics and spectral responsivity were measured using an HP4142B DC Source/Monitor (full-scale range from 10^{-15} A to 1 A and a resolution of 10^{-13} A). A 100 W quartz tungsten halogen lamp with a monochromator TRIAX-180 (1200 g/mm grating with a spectral dispersion of 3.6 nm/mm and a spectral resolution of 0.3 nm at 546 nm), was used as light source. A collimator lens was used to image the light on the entrance slit. At the exit slit, a pinhole and a focusing lens were used to achieve a beam with a diameter of about 400 μm . The monochromator, optical hardware and the microspectrometer were assembled and aligned

on an optical table. Without focusing lens, the output beam coming from the monochromator illuminates the complete etalons array. Using the pinhole, focusing lens and controlling the distance to the microspectrometer it is possible to illuminate only one etalon. A translation mount was used for exact positioning of the microspectrometer in the vertical, horizontal and depth planes in order to scan all etalons. The measurements were calibrated with a commercially available photodiode, Hamamatsu S1336-5BQ.

System operation is demonstrated in a limited range using a 16-channel micro-spectrometer designed for operation in the spectral range between 400 to 500 nm with inter-channel shift of about 6 nm. Each of the channels consists of a 20 nm-Al / SiO₂ / 45 nm-Ag layer stack, where the oxide layer thickness changes between 225 nm and 300 nm with 5 nm steps.

Optical spectral measurements in reflectance (using an external detector, Leica Microscope Photometer System) show that each of the channels is sensitive to only one narrow spectral band. Independent measurements were performed on a cavity of thickness 1000 nm. These results indicate a FWHM of 6 nm and a finesse of 12 (see Fig. 10).

Subsequently, measurements were performed on the device with integrated photodiodes. A dark current of 0.2 pA at 0 V and 1 pA at -4 V (see table 1) was measured for a square photodiode with an active area of 1 mm². The photocurrent measured in a normal channel at the same conditions is 10 μA @ -4 V. The dark current directly limits the Signal Noise Ratio (SNR takes into account the noise due to: photon, photoelectron and gain). The photocurrent, at a given source spectral power, is the result of a trade-off between sensitivity, selectivity, and the number of channels used. An increased Ag-layer thickness improves selectivity but causes higher absorption losses and low sensitivity and thus decreases SNR. The presence of the Fabry-Perot filter limits the light transmitted to the underlying photodiode to less than 15% of the incident light. Atomic force microscope (AFM) was employed to examine the surface morphology of the realized Fabry-Perot structures. The RMS roughness of the surface mirror in the array-type micro-

spectrometer is typically 15 nm (see Fig. 11). A possible explanation for the high value can be the back etching applied to the PECVD oxide in order to define the cavity gap.

Fig. 12 presents the spectral responsivity (A/W) between 400 nm to 800 nm for all 16 channels using on-chip photodiodes. The ratio between the base line and the peak maximum ranges from 4 to 7. The relatively high stray light, beam divergence and the roughness surface are responsible for the background signal. Stray-light compensation methods must be used in order to compensate for the non-idealities of both the incident light beam and the Fabry-Perot etalon.

A solution to this problem is to use a compensation structure. It consists of the same layer stack as used in any of the active channels. The difference is that the optical length of the cavity is decreased below $\lambda/10$ (<40 nm if applied for measurements in the visible spectral range). This excludes any resonance inside the cavity. However, the parasitic signal caused by stray-light transmittance is similar to that of the active channel and can be used for compensation. Photodiodes are integrated underneath both the active and the compensating device and after subtraction of the photocurrents a compensated signal results. It should be mentioned that the conventionally used dark current compensation (an opaque layer deposited on top of a photodetector) compensates only for the non-idealities (dark current) of the detector itself. This method, in contrary, compensates for the non-idealities of detector, Fabry-Perot filter and incident light beam at the same time. After photocurrent subtraction, the average background signal level is decreased by a factor of 10 and, as a consequence, the spectral selectivity of the device is increased.

V. CONCLUSIONS

A single-chip spectrometer, using Fabry-Perot resonance cavities on a distributed photodetectors array, was fabricated and characterized (see Table 1). The advantage of the device presented is that it can easily be tuned during fabrication to cover different spectral bands, by adjusting

the etching time only, without affecting the device layout. Such a device is extremely suitable for applications in microsystems, because of its small size, high spectral selectivity, and low cost. Microspectrometers for the UV and IR are also feasible with this technique using dielectric mirrors.

The performance of the array-type microspectrometer presented is compared with that of a low-cost spectrometer [17] and with a commercially available spectrometer, (Spectronic 20) [18] (see Table 2). Both spectrometers are based on a grating element and use a CCD detector. The free spectral range in the array-type device is limited by the low quantum efficiency of the photodiodes at low wavelengths. The high resolution in Fabry-Perot based spectrometers is obtained for high interference orders. In our case a resolution of 222 is achieved in fourth mode (four peaks obtained). But for a single peak, first mode, a reasonable resolution of 25 was measured.

The technique used for fabrication of the Fabry-Perot etalons allows, for simple expansion of the number of channels to 64 or 128, to increase the operation range in the visible part of the spectrum and to 512 or 1024 in order to cover a wide range inclusive ultraviolet and far infrared. The minimum value reproducible and controllable in the difference at the SiO₂ film thickness between two different channels is 2 nm using the Reactive Ion Etching (RIE) process to etch the SiO₂ layer.

ACKNOWLEDGMENTS

The authors would like to thank the staff of Delft Institute of Microelectronics and Submicron Technology (DIMES), especially J. Groeneweg, for technical assistance in fabrication of the devices. This work is supported in part by STW (project DEL 55.3733), TUDelft and FCT-Portugal (Program Praxis XXI-BD/5181/95).

REFERENCES

- [1] J. H. Correia, M. Bartek, R. F. Wolffenbuttel, "High-selectivity single-chip spectrometer for operation at visible wavelengths," Proc. of IEDM'98, S. Francisco, USA, pp. 467-470, 1998.
- [2] J. D. Patterson and B. van Zeghbroeck, "Fabrication and analysis of Si/SiO₂ Micro-mechanical Modulators," Digest IEEE/LEOS 1996 Summer topical meeting on optical MEMS and their applications, pp. 25-26, 1996.
- [3] T. A. Kwa, P.M.Sarro, R.F. Wolffenbuttel, "Backside-illuminated silicon photodiode array for an integrated spectrometer," IEEE Transactions on Electron Devices, Vol. 44, No. 5, pp.761-765, May 1997.
- [4] N.F. Raley, D.R. Ciarlo, J.C. Koo, B. Beiriger, J. Trujillo, C. Yu, G. Lomis, R. Chow, "A Fabry-Perot Microinterferometer for Visible Wavelength," Proc. 5th IEEE Solid State Sensor and Actuator Workshop, Hilton Head Island, SC, USA, pp. 170-173, 1992.
- [5] J. H. Correia, M. Bartek, R. F. Wolffenbuttel, "Bulk-micromachined tunable Fabry-Perot microinterferometer for the visible spectral range," Proc. of Eurosensors XII, Southampton, UK, pp.287-290, September 1998.
- [6] A. T. T. D. Tran, Y. H. Lo, Z. H. Zhu, D. Haronian, E. Mozdy, "Surface micromachined Fabry-Perot tunable filter," IEEE Photonics Technology Letters, Vol. 8-3, pp. 393-395, 1996.
- [7] R. T. Carline, D. A. O. Hope, D. J. Robbins, M. B. Stanaway, "Vertical cavity longwave infrared SiGe/Si photodetector using a buried silicide mirror," Proc. of IEDM'97, Washington, USA, 1997.
- [8] S. D. Senturia, Narayan Aluru, J. White, "Simulating the behavior of MEMS devices: computational methods and needs," IEEE Computational Science & Engineering, pp. 30-43, March 1997.

- [9] D.P. Poenar, R.F. Wolffenbuttel, "Optical properties of thin-film silicon-compatible materials," *Applied Optics*, Vol. 36, No. 21, pp. 5122-5128, July 1997.
- [10] R. F. Wolffenbuttel, "Photodiodes in silicon with an electrically-programmable UV response," *Sensors and Actuators A*, A22, pp. 559-563, 1990.
- [11] H.A. Macleod, "Thin-film optical filters," Adam Hilger Ltd, 2nd edition, 1986.
- [12] D.-Y. Song, R. W. Sprague, H. A. Macleod, M. Jacobson, "Progress in the development of a durable silver-based high-reflectance coating for astronomical telescopes," *Appl. Optics*, Vol. 24, No. 8, pp. 1164-1170, 1985.
- [13] C. Cusatis, "Handbook of applied photometry," American Institute of Physics Press, 1997.
- [14] B. Fowler, "CMOS area image sensors with pixel level A/D conversion," Ph.D. thesis, Stanford University, 1995.
- [15] C. Wang, Y. Ni, F. Devos, "A spatio-temporal differentiation light sensor," *Sensors and Actuators A*, A62, pp. 492-495, 1997.
- [16] R. S. Muller, T. I. Kamis, "Device electronics for integrated circuits," John Wiley & Sons, 1986.
- [17] G. M. Yee, N. I. Maluf, P. A. Hing, M. Albin, G. T. A. Kovacs, "Miniature spectrometers for biochemical analysis," *Sensors and Actuators A*, 58, pp.61-66, 1997.
- [18] Milton Roy/Spectronic Instruments Inc., Data catalog, Rochester, New York, 1997.

List of Figures

1. Schematic structure of the microspectrometer. One individual channel is shown in cross section.

2. A 4x4 array microspectrometer in perspective. Each of the Fabry-Perot cavities is tuned to transmit in different spectral band.
3. Reflectance of Ag, Au and Al as a function of radiation wavelength [10].
4. Transmittance and finesse as a function of silver thickness.
5. Simulated transmittance vs. wavelengths for 60 nm Ag/ 1000 nm SiO₂/ 60 nm Al layer stack. Fourth mode of operation (four peaks achieved). The different values of transmittance depends on the optical properties of the materials used.
6. Principle used for fabricating a 4x4 array microspectrometer. After the deposition of the silicon dioxide, each mask is used with a different etch time. In this example the first mask will etch one half of whole thickness, the second one fourth, etc.
7. Post bipolar processing fabrication sequence.
8. SEM photograph showing the cross-section of one of the channels.
9. Photograph of the fabricated microspectrometer with 4x4 channels. The die area is 4.7x4.7 mm².
10. Measured reflectance vs. wavelength for a 45 nm/ 1000 nm SiO₂/ 20 nm Al layer stack.
11. AFM surface scan of a 45 nm Ag /300 nm PECVD oxide/20 nm Al/250 thermal-oxide layer stack (array-type device mirror surface).
12. Spectral responsivity of the 16-channel micro-spectrometer for a 45 nm Ag / SiO₂/ 20 nm Al layer stack. The SiO₂ layer thickness is used as a parameter and changes from 225 nm to 300 nm in 5 nm increments.

List of Tables

Table 1: Electrical and optical characteristics.

Table 2: Array-type spectrometers performance comparison.

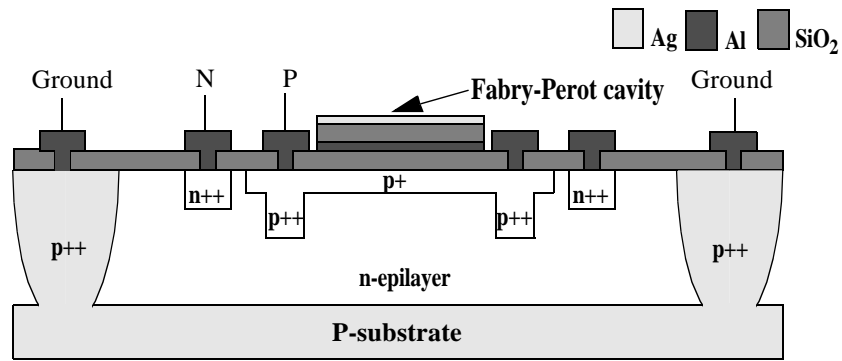


Fig. 1: Schematic structure of the microspectrometer. One individual channel is shown in cross section.



Fig. 2: A 4x4 array microspectrometer in perspective. Each of the Fabry-Perot cavities is tuned to transmit in different spectral band.



Fig. 3: Reflectance of Ag, Au and Al as a function of radiation wavelength [10].

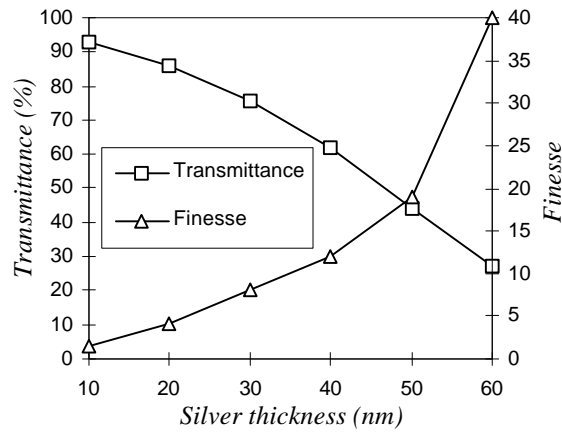


Fig. 4: Transmittance and finesse as a function of silver thickness.

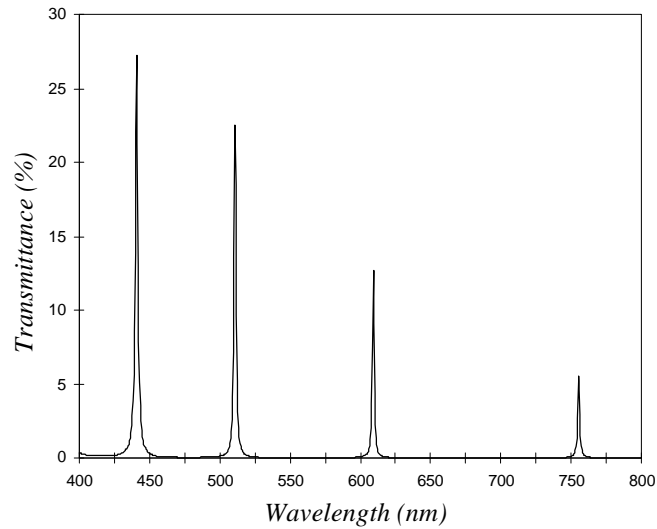


Fig. 5: Simulated transmittance vs. wavelengths for 60 nm Ag/ 1000 nm SiO₂/ 60 nm Al layer stack. Fourth mode of operation (four peaks achieved). The different values of transmittance depends on the optical properties of the materials used.

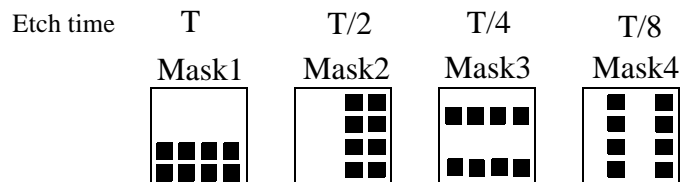


Fig. 6: Principle used for fabricating a 4x4 array microspectrometer. After the deposition of the silicon dioxide, each mask is used with a different etch time. In this example the first mask will etch one half of whole thickness, the second one fourth, etc.

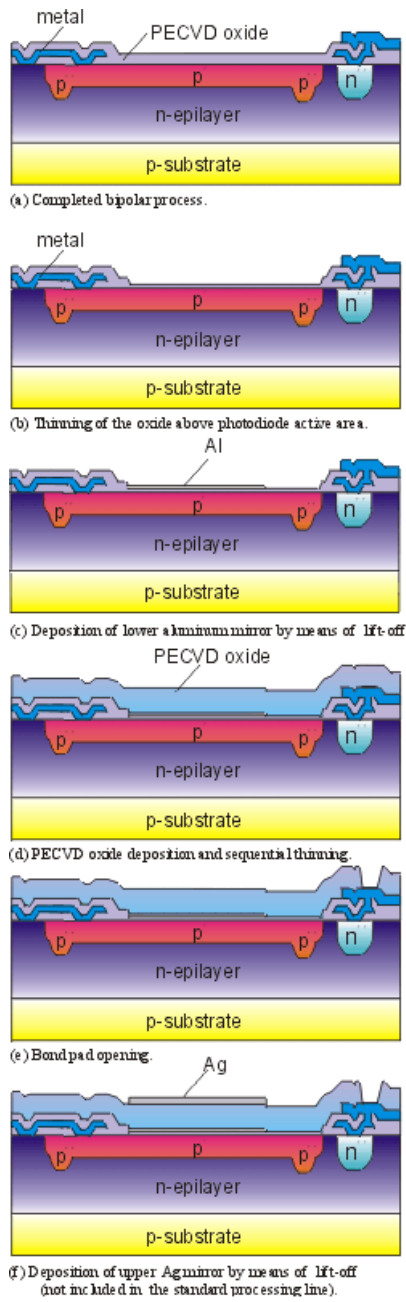


Fig. 7: Post bipolar processing fabrication sequence.

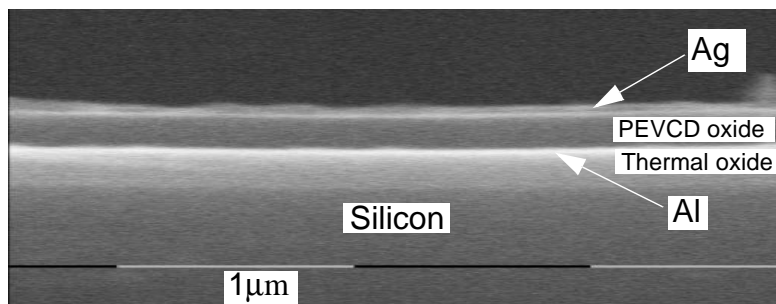


Fig. 8: SEM photograph showing the cross-section of one of the channels.

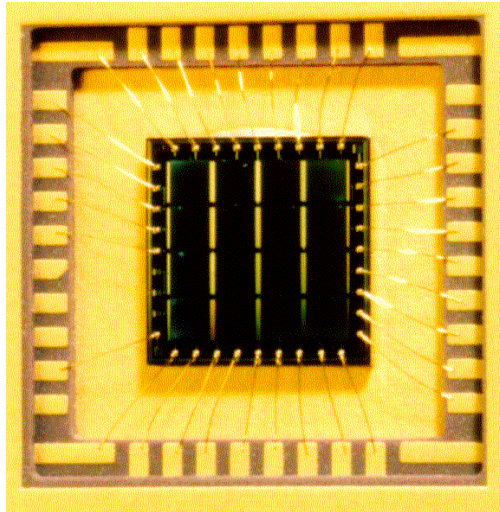


Fig. 9: Photograph of the fabricated microspectrometer with 4x4 channels. The die area is $4.7 \times 4.7 \text{ mm}^2$.

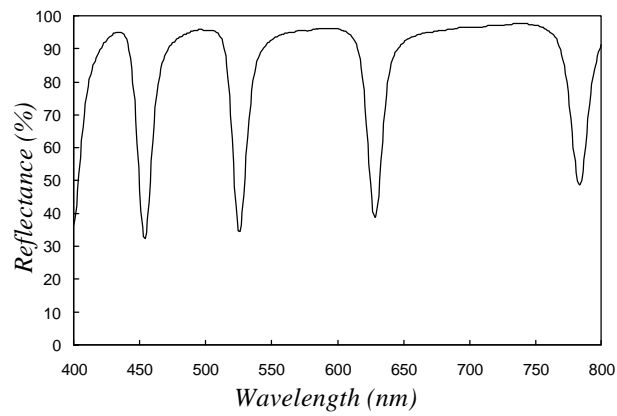


Fig. 10: Measured reflectance vs. wavelength for a 45 nm Ag / 1000 nm SiO_2 / 20 nm Al layer stack.

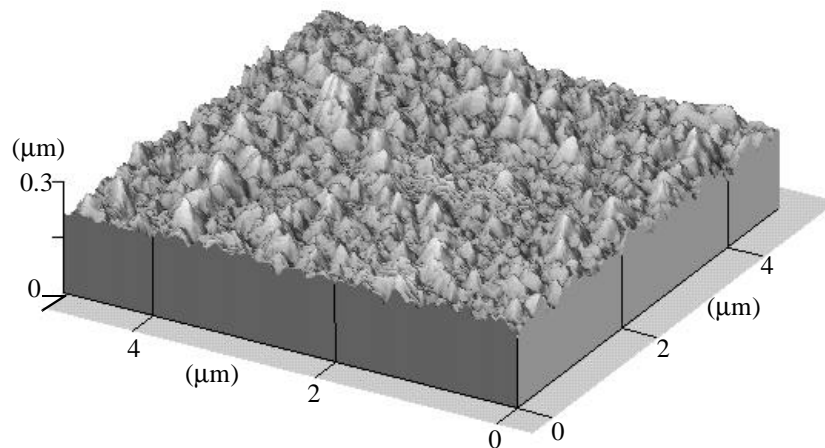


Fig. 11: AFM surface scan of a 45 nm Ag / 300 nm PECVD oxide / 20 nm Al / 250 nm thermal-oxide layer stack (array-type device mirror surface).

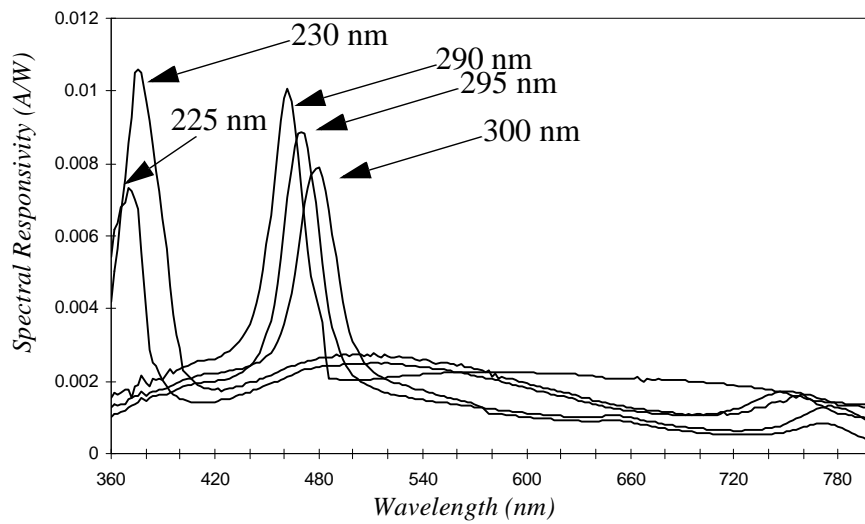


Fig. 12: Spectral responsivity of some channels of the 16-channel microspectrometer for a 45 nm Ag / SiO₂ / 20 nm Al layer stack. The SiO₂ layer thickness is used as a parameter and changes from 225 nm to 300 nm in 5 nm increments.

Tables:

Table 1 Electrical and optical characteristics

Feature	Result
Technology	Bipolar
Device area	4.7 x 4.7 mm ²
FWHM @t _{SiO2} =300 nm	16 nm
Finesse @t _{SiO2} =300 nm	Single peak
FWHM (simulated) @60 nm Ag mirrors @t _{SiO2} =1 μm	1.8 nm
Finesse (simulated) @60 nm Ag mirrors @t _{SiO2} =1 μm	40
Dark current@ 0 V	0.2 pA
Dark current@ -4 V	1 pA
Spectral response maximum @-4V	0.013 A/W@388 nm
Incident angle range	±10 °

Table 2 Array-type spectrometers performance comparison.

	FWHM (nm)	FSR (nm)	Accuracy (nm)	Resolution	Dispersive element
Array type (this work)	16 1.8	400-520 400-472	±3	25* 222**	FP etalon
Low-cost Spectr.[15]	9.1 @632.8	450-750	2.55	69.8	Grating
Spectronic 20 [16]	20	340-950	±2.5	47.5 @950 nm	Grating

*First mode operation (single-peak). **Fourth mode operation (four peaks) and $R=\lambda/\text{FWHM}$.